Mon. Not. R. Astron. Soc. **388,** 1305–1313 (2008) doi:10.1111/j.1365-2966.2008.13489.x

A potential new method for determining the temperature of cool stars

S. Viti,[1⋆] H. R. A. Jones,[2] M. J. Richter,[3] R. J. Barber,[1] J. Tennyson[1] and J. H. Lacy[4]

[1]*Department of Physics and Astronomy, University College London, Gower Street, London WC1E 6BT*
[2]*Centre for Astrophysics Research, University of Hertfordshire, College Lane, Hatfield AL10 9AB*
[3]*Physics Department, UC Davis, One Shields Avenue, Davis, CA 95616, USA*
[4]*Department of Astronomy, University of Texas at Austin, 1 University Station, Austin, TX 78712, USA*

Accepted 2008 May 16. Received 2008 May 16; in original form 2007 December 27

ABSTRACT

We present high-resolution ($R = 90\,000$) mid-infrared spectra of M dwarfs. The mid-infrared region of the spectra of cool low-mass stars contains pure rotational water vapour transitions that may provide us with a new methodology in the determination of the effective temperatures for low-mass stars. We identify and assign water transitions in these spectra and determine how sensitive each pure rotational water transition is to small (25 K) changes in effective temperature. We find that, of the 36 confirmed and assigned pure rotational water transitions, at least 10 should be sensitive enough to be used as temperature indicators.

Key words: stars: atmospheres – stars: fundamental parameters – stars: low-mass, brown dwarfs – infrared: stars.

1 INTRODUCTION

Low-mass stars (LMS) constitute ∼80 per cent of our stellar neighbourhood. They provide a probe of our understanding of main-sequence stellar evolution and are key in determining the boundary between stellar and sub-stellar objects. However, their spectra are extremely rich in structure and their opacity is made up of many molecular and atomic absorbers, each with hundred of thousands to millions of spectral lines. This means that colours are not easily interpretable as diagnostic of their properties. Among the fundamental properties of LMS, of particular importance is their effective temperature, $T_{\rm eff}$: the latter has frequently been investigated but it is still not well determined. In particular, there is not yet a tight correlation between spectral type and effective temperature as there has been a longstanding discrepancy between empirical effective temperatures and those derived by synthetic spectra (up to 500 K as discussed by Jones et al. 1996). This is primarily due to the lack of a complete inclusion of molecular and atomic opacities in the models, in particular in the near-infrared (NIR). Modelling the atmosphere of LMS in the NIR is not a trivial task: water vapour dominates this part of the spectrum and at the effective temperature applicable to cool star atmospheres (<4000 K) water can access energies as high as 45 000 cm^{-1} before it dissociates; to reproduce high-temperature water spectra is very challenging because of the complexity of the vibrational and rotational motion of asymmetric triatomic molecules. Leggett et al. (2000, 2001) used a synthetic grid which includes the water linelist calculated by Partridge & Schwenke (1997) to determine fundamental parameters for a large sample of LMS. They conclude that problems remain with the match of the observed water bands. Allard, Hauschildt & Schwenke (2000) also find that the models including this water linelist reproduce well late-type dwarfs but fail to reproduce hotter dwarfs. The main sources of error in present water opacity data bases are the incorrect high-temperature transitions (Jones et al. 2002, 2005).

Recently, a new water linelist, BT2, has been produced (Barber et al. 2006). The BT2 linelist is by far the most complete linelist available, reaching higher energies than previously published. A comparison between a previous release of the BT2 linelist (BT1) and the PS linelist showed that at higher temperatures ($T > 2000$ K) the PS linelist is missing around 25 per cent of the water vapour opacity (Jones et al. 2005). While the BT2 increases the accuracy of the fitting in the NIR region, its cut-off at energies above 30 000 cm^{-1} still means that none of the energy levels above 20 000 cm^{-1} is capable of being excited by 1 μm photons (Barber et al. 2006).

Although the strongest water vapour opacity is at shorter wavelengths, the analysis of sunspots (Wallace et al. 1995) shows that H_2O also accounts for the majority of lines in the mid-infrared (MIR) region between 8 and 21 μm. Polyansky et al. (1997a,b) successfully assigned many of the water transitions in the 10–13 μm spectra of sunspots with further recent assignments being made in conjunction with the analysis of oxy-acetylene emission spectra (Coheur et al. 2005; Zobov et al. 2006). In this spectral region, the water transitions are largely pure rotational, in contrast to the vibration–rotation transitions which dominate at shorter wavelengths. The use of pure rotational transitions greatly simplifies the spectral analysis as estimates of the transition strengths are much more straightforward. To a good approximation, the strength of individual rotational transitions can be estimated from a simple algebraic formula times a Boltzmann factor. Furthermore, the presence of pure rotational transitions within different vibrational

⋆E-mail: sv@star.ucl.ac.uk

states, which is characteristic of the sunspot spectrum, yields a large dynamic range for the temperature analysis. These advantages potentially make the MIR region ideal for the determination of the effective temperature scale for LMS.

Here, we propose a new methodology for establishing the effective temperatures of cool stars, in particular LMS, based on high-resolution MIR spectroscopy. Taking advantage of the relatively easy to interpret MIR spectrum in cool stars has been done before: Ryde et al. (2006) used high-resolution observations of water vapour in super-giants to show that classical photosphere models cannot fit the observed spectra and that synthetic spectra based on cooler photospheric temperature structure are needed. This supports the idea that individual rotational water lines are highly sensitive to temperature variations in this region. In this paper, we present the *first* high-resolution (90 000) MIR observational data for two M dwarfs, together with one M giant. Our observations are described in Section 2. In Section 3, we present the data, the identification of the water lines and a theoretical sensitivity study using the BT2 linelist. In Section 4 we briefly conclude.

2 OBSERVATIONS

The data were taken in 2006 November using the Texas Echelon-Cross-Echelle Spectrograph (TEXES; Lacy et al. 2002) at the Gemini North 8-m telescope. The observations were made on the nights of November 20, 23 and 27 for a total of ∼13 h. We observed three objects (BS587, GJ411 and GJ273 – see Table 1) in the TEXES high spectral-resolution mode in two grating positions: 11.2 and 12.5 μm (800 and 892.857 cm^{-1}). The two grating positions were chosen on the basis of a relative lack of narrow telluric features and the abundance of temperature-sensitive water features based on an early version of our ab initio water line list, as well as a careful analysis of the sunspot ($T \sim 3300$ K) 10–13 μm spectrum. The spectral coverage was 0.5 per cent at 11.2 μm and 0.75 per cent at

Table 1. Properties of objects.

Object	RA	Dec.	Sp.	d (pc)	v_{rad} (km s^{-1})	M_{bol}	T_{eff}(K)	log g
GJ411[1]	11 03 20.2	+35 58 11.5	M2V	2.52	−84.74	8.88	3510	5
BS587[2]	02 00 26.8	−08 31 25.9	M4.6III	182	+12.70		3425	−1
GJ273[3]	07:27:24.5	+05:13:32.5	M3.5V	3.76	+18.10	9.56	3150	5

[1]Effective temperature taken from Tsuji et al. (1996); surface gravity from Jones et al. (1996); M_{bol} from Cushing, Rayner & Vacca (2005).
[2]Effective temperature taken from van Belle et al. (1999); surface gravity from Fluks et al. (1994).
[3]Effective temperature taken from Tsuji et al. (1996); surface gravity from Jones et al. (1996) and M_{bol} from Delfosse et al. (1998).

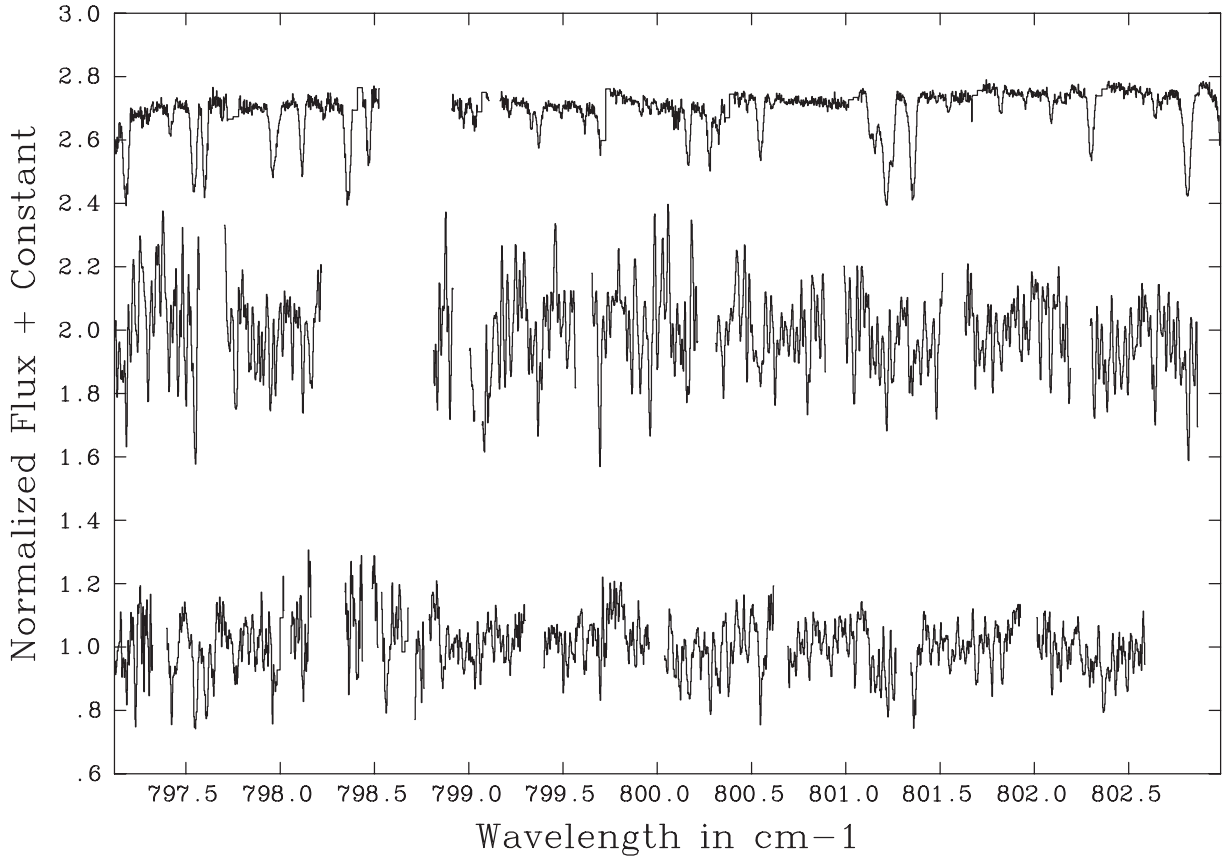

Figure 1. Observed spectra centred at 11.2 μm. Top: BS587, middle: GJ273 and bottom: GJ411. Spectra have been corrected for stellar velocities (see text).

12.5 μm. At 12.5 μm, there are slight gaps in the spectral coverage because the angular width of the spectral orders is larger than the detector. The spectral resolution, as determined by Gaussian fits to telluric atmospheric lines in the 12.5 μm setting, has a full width at half-maximum (FWHM) equivalent to $R = 90\,000$. We expect the same spectral resolution at 11.2 μm. The slit width was 0.5 arcsec for all observations and the length was roughly 4 and 2.5 arcsec at 11.2 and 12.5 μm, respectively. For all observations, we nodded the source along the slit roughly every 10 s.

Of our targets, GJ411 and BS587 were sufficiently bright to fine-tune pointing based on the signal recorded from every nod pair. GJ273 was weaker and required accumulation of several nod pairs to evaluate pointing adjustments with confidence. On November 23, clouds were occasionally present based on elevated background signal through TEXES. We discarded the data that were most severely affected.

Coordinates and properties of the three objects are listed in Table 1. The two dwarfs were chosen among a sample of well-studied dwarfs: note that for both GJ411 and GJ273, the quoted temperatures have uncertainties of at least 100 K (cf. Tsuji, Ohnaka & Aoki 1996). The quoted radial velocities are from the literature (Marcy, Lindsay & Wilson 1987) and they match the sunspot features within 0.5 km s^{-1}.

The data were reduced according to standard procedures as described in Lacy et al. (2002). The TEXES pipeline provides for differencing of individual nod pairs, correcting spikes and cosmic rays, establishing a wavelength scale based on a user-identified telluric line, correcting distortions in the instrument, extracting 1D spectra using optimal weighting along the slit length and combining spectra from the same night weighted by the square of their signal-to-noise ratio (S/N). The pipeline also performs flat-fielding and a first-order correction for telluric spectral features using the difference between an ambient temperature blackbody and sky emission. Further flat-field and telluric correction comes from the division by a featureless point source such as an asteroid or hot star. Data from separate nights were aligned spectrally and combined according to the square of their S/N using custom Interactive Data Language procedures. The dispersion calculations are accurate to 0.6 km s^{-1} or better.

3 ANALYSIS

Figs 1 and 2 show the recorded spectra for our sample for the two wavelength regions. The gaps in the spectra coincide with the removals of bad pixels and of telluric lines. The S/N varies from star to star (∼100 for BS587, 40 for GJ411 and five for GJ273). We used the bright star BS587 as a template for the identification of the water lines in the spectra due to its high S/N. In total, we identified 71 lines in the observed spectra which could potentially be water (see Table 2); however, only 52 of them are confirmed by comparison with the BT2 linelist (see Table 2 and Figs 3 and 4). Some of these (24, 25, 29, 38, 44, 53, 62 and 66 in Table 2) are weak according to theory. Note that in order for a feature to be confirmed and assigned as water, we required its intensity to be $>10^{-23}$ cm^{-1} molecule and its frequency to be within 0.001 cm^{-1}. 40 of the 52 lines have been independently identified and assigned in the sunspot spectra (Zobov et al. 2006). Of the 19 remaining lines not identified in BT2, 13

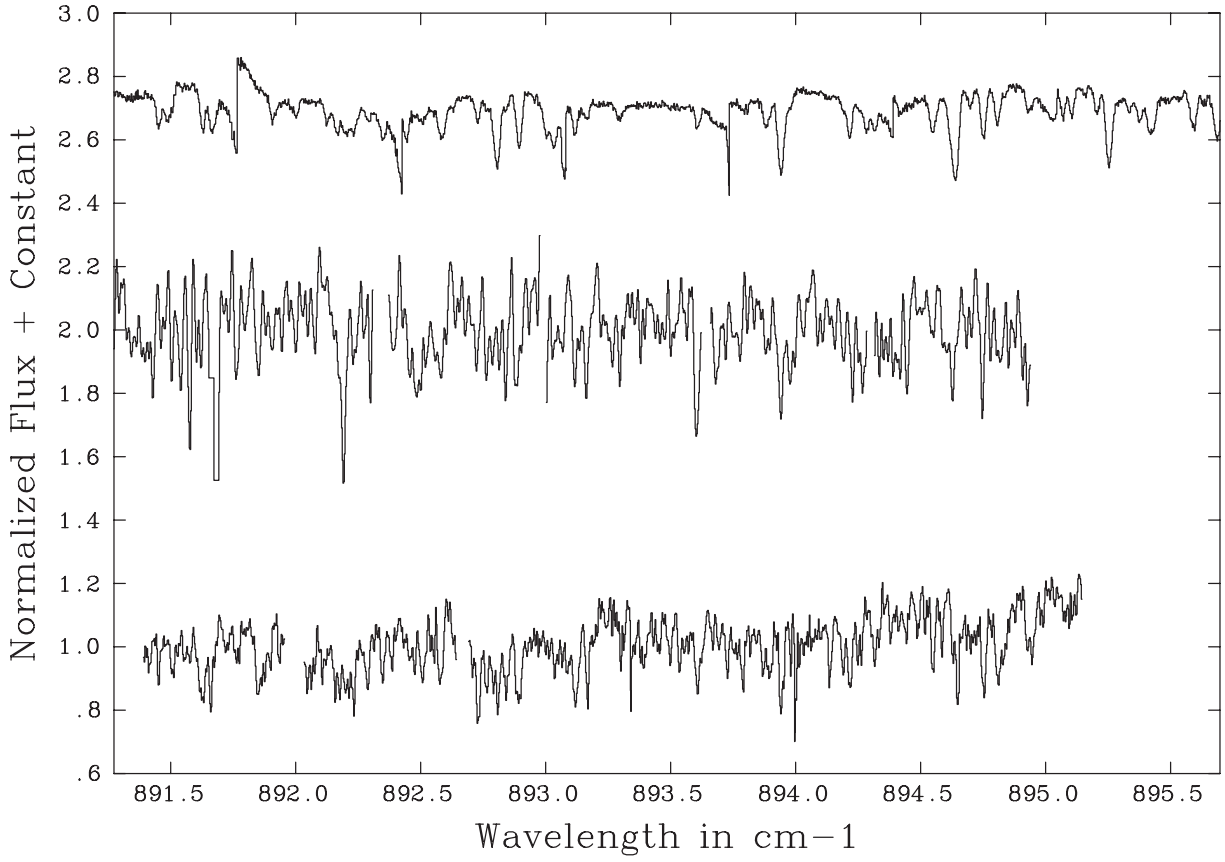

Figure 2. As for Fig. 1 for the 12.5 μm region.

Table 2. Transitions identified in the observed spectra of BS587. The confirmed water transitions are also given with energy levels, and quantum assignments when known experimentally. Transitions in italic are experimentally unknown transitions. The 10th column (sunspot) states whether the confirmed water transition has been independently identified in sunspots (Y) or not (N). The last column is the temperature of the maximum intensity gradient within the 1500 to 4000 K limits of our chosen model grid (see Section 4).

	Frequency (cm^{-1})	$\nu_1\nu_2\nu_3$ (u)	J (u)	$K_a\,K_c$ (u)	$\nu_1\nu_2\nu_3$ (l)	J (l)	$K_a\,K_c$ (l)	E(l)	Sunspot	T_{max} (K)
1	797.130[1]	100	18	7 12	100	17	4 13	7597.8219	Y	1500
2	797.188	000	24	11 14	000	23	10 13	7927.6588	Y	1500
3	797.272								Y	
4	797.301								Y	
5	797.424	011	21	20 2	011	20	19 1	14390.7454	Y	3225
6	797.551	010	20	17 4	010	19	16 3	9559.7822	Y	1500
7	797.693								Y	
8	797.966	020	20	13 8	010	19	18 1	10174.6070	Y	1500
9	798.122	000	23	12 12	000	22	11 11	7656.5656	Y	1500
10	*798.239*		*23*			*22*		*12650.7318*	N	*2925*
11	*799.227*		*22*			*21*		*18066.4172*	N	*3875*
12	799.333[1]	011	21	19 3	011	20	18 2	14106.5900	Y	3175
13	*799.359*		*21*			*20*		*14106.5958*	N	*3175*
14	*799.372*		*22*			*21*		*12732.1876*	Y	*2925*
15	*799.493*		*25*			*24*		*15580.8988*	N	*3425*
16	*799.614*		*21*			*20*		*14671.8932*	Y	*3275*
17	*799.790*		*20*			*19*		*17771.2525*	N	*3800*
18	799.919	011	23	12 12	011	22	11 11	13031.5180	Y	2975
19	799.968[1]	010	13	7 7	010	12	4 8	3843.4105	Y	1500
20	800.105								N	
21	800.169	100	22	16 7	100	21	15 6	11774.0830	Y	2750
22	800.229								Y	
23	800.280	000	24	9 15	000	23	8 16	7459.6821	Y	1500
24	800.321	020	18	11 8	100	17	10 7	8608.2236	Y	1500
25	800.427	100	25	11 15	100	24	10 14	11962.4012	Y	2800
26	800.435								N	
27	800.476								Y	
28	800.552	100	24	12 13	100	23	11 12	11674.6517	Y	2750
29	800.611	020	34	2 33	020	34	1 34	14127.8724	N	3175
30	801.132	001	22	17 6	001	21	16 5	12109.9259	Y	2825
31	801.159	001	22	22 1	001	21	21 0	13486.1810	Y	3075
32	801.219	000	21	17 4	000	20	16 5	8100.2905	Y	1500
33	801.252	000	24	11 13	000	23	10 14	7924.4497	Y	1500
34	801.360	000	21	21 0	000	20	20 1	9257.4587	Y	1500
35	801.546								Y	
36	*802.654*		*22*		*011*	*21*	*13 9*	*13104.6565*	*N*	*3000*
37	892.122								Y	
38	892.160	100	27	11 16	001	26	9 17	13034.8501	N	2975
39	892.198	010	26	13 13	010	25	12 14	11398.7613	Y	1500
40	892.228	010	25	25 0	010	24	24 1	14644.7869	Y	3275
41	892.286	000	29	12 18	000	28	11 17	11087.9927	Y	1500
42	892.345	030	16	5 12	030	15	2 13	7690.7488	Y	1500
43	892.507								Y	
44	892.578	001	26	23 3	001	25	22 4	16039.7119	Y	3515
45	892.634	001	27	16 12	001	26	15 11	14531.6796	Y	3250
46	892.724	100	26	19 8	100	25	18 7	14815.6577	Y	3300
47	892.760	100	26	23 4	100	25	22 3	16021.8356	Y	3500
48	892.805	000	25	23 2	000	24	22 3	12049.8071	Y	2800
49	892.838	001	26	20 6	001	25	19 7	15161.0169	Y	3350
50	*892.871*		*26*			*25*		*18864.6094*	*N*	*4000*
51	892.891	010	25	15 10	010	24	14 11	11478.5602	Y	1500
52	893.937	000	25	19 6	000	24	18 7	10831.4717	Y	1500
53	894.184	020	31	0 31	010	31	1 30	11439.9008	Y	1500
54	894.214	010	27	12 15	010	26	11 16	11673.7867	Y	2750
55	*894.283*		*26*			*25*		*18588.1034*	*N*	*3950*
56	894.416								N	
57	894.542	010	19	7 13	010	18	4 14	6095.5140	Y	1500
58	894.637	000	20	8 13	000	19	5 14	5052.6689	Y	1500
59	*894.697*		*29*			*28*		*19917.3223*	*N*	*4000*
60	894.746	010	23	7 16	010	22	6 17	8181.3570	Y	1500
61	894.806	020	24	15 10	020	23	14 9	12832.5041	Y	2950
62	894.920	100	18	4 15	100	17	1 16	6885.4857	Y	1500

Table 2 – *continued*

	Frequency (cm^{-1})	$\nu_1\nu_2\nu_3$ (u)	J (u)	$K_a\,K_c$ (u)	$\nu_1\nu_2\nu_3$ (l)	J (l)	$K_a\,K_c$ (l)	E(l)	Sunspot	T_{max} (K)
63	895.026								N	
64	895.070								Y	
65	*895.094*		*22*			*21*		*15222.2697*	*N*	*3375*
66	895.154	100	20	8 13	100	19	5 14	8618.8825	Y	1500
67	895.203	001	20	5 15	001	19	4 16	8286.0153	Y	1500
68	895.252	000	25	22 3	000	24	21 4	11756.8965	Y	2750
69	895.335								N	
70	895.376								N	
71	895.423[1]	100	13	9 5	100	12	6 6	6051.2728	Y	3375

[1]Assigned by Zobov et al. (private communications) in the sunspots.

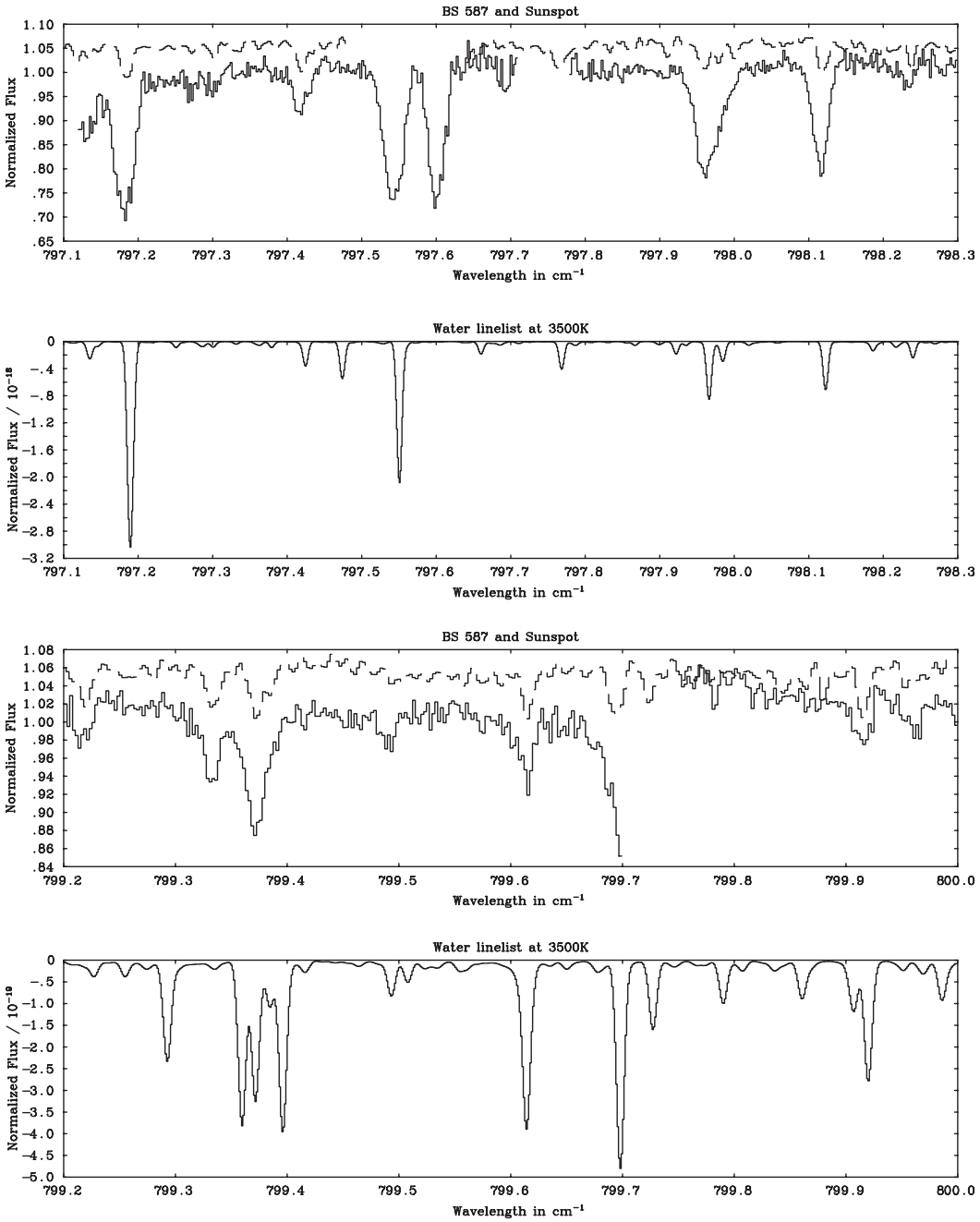

Figure 3. Selected portions of spectra in the 11.2 μm region. Top: BS587 (Continuous) overplotted to the sunspot spectrum (dashed, flux offset by +0.05 for clarity). Bottom: synthetic BT2 linelist computed at 3500 K.

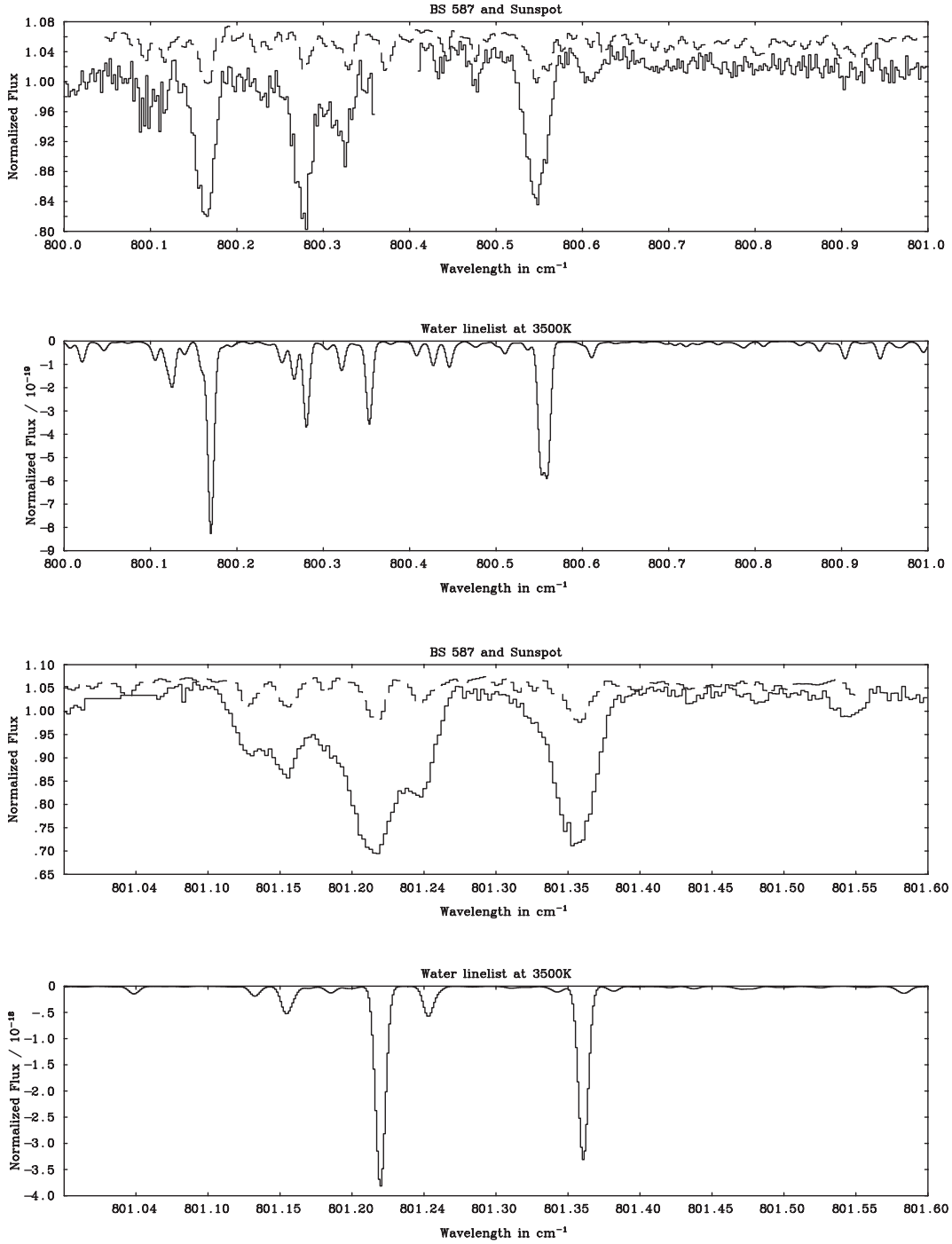

Figure 4. As in Fig. 3 but for the 12.5 μm region.

are also present in the sunspot spectra (Wallace et al. 1995) and four of these 13 have been in fact assigned to water (Zobov et al. 2006; Zobov, private communications). Many of the observed features are blends of multiple lines (often two, the para:ortho pair lines): for these cases, we assigned the band to the strongest component (ortho in the case of pairs of lines).

Figs 3 and 4 show examples of our line assignment with the observed stellar spectrum on the top panel overplotted to the sunspot spectrum (offset from the BS587 spectrum by +0.05), and with a synthetic water linelist computed at 3500 K on the bottom panel. Note that the choice of temperature for the synthetic water spectrum is *not* a best fit but was chosen to represent a bright cool stellar atmosphere and is close to that of the sunspot spectrum. In fact, a synthetic spectrum at 3000 K may be more representative of a 3500 K giant since the gas temperatures of the layers where most flux is emitted are typically 500 K less than the effective temperature of the star (Allard et al. 1997). We have compared a 3000 K synthetic water linelist with BS587 and found that the same number of water lines are identified.

Some of the lines identified as water transitions in the observed spectra are not from experimentally known levels. For some of these cases, the quantum numbers have not been fully determined

Table 3. Relative intensity of pure rotational and assigned water lines at 3500 K (Column 3), and Gradient at 3500 K (Column 4).

	Frequency (cm^{-1})	Intensity (3500 K)	Gradient (3500 K)
2	797.188	5.97E-21	9.48E-26
5	797.424	4.19E-22	3.24E-25
6	797.551	3.05E-21	6.36E-25
9	798.122	6.68E-21	1.08E-25
18	799.919	7.33E-22	4.51E-25
21	800.169	1.23E-21	5.75E-25
23	800.280	7.24E-21	2.86E-25
25	800.427	1.14E-21	5.58E-25
28	800.552	1.28E-21	5.84E-25
29	800.611	4.67E-22	3.47E-25
30	801.132	1.07E-21	5.43E-25
31	801.159	6.08E-22	4.06E-25
32	801.219	5.56E-21	2.02E-25
33	801.252	5.98E-21	9.27E-26
34	801.360	3.46E-21	5.98E-25
39	892.199	1.43E-21	6.08E-25
40	892.228	3.78E-22	3.03E-25
41	892.286	1.63E-21	6.32E-25
42	892.345	6.58E-21	8.00E-26
44	892.578	2.13E-22	2.05E-25
45	892.634	3.96E-22	3.12E-25
46	892.724	3.52E-22	2.89E-25
47	892.760	2.14E-22	2.06E-25
48	892.805	1.10E-21	5.49E-25
49	892.838	3.05E-22	2.63E-25
51	892.891	1.39E-21	8.59E-26
52	893.937	1.81E-21	6.48E-25
54	894.214	1.28E-21	5.85E-25
57	894.542	1.27E-20	2.55E-24
58	894.637	1.95E-20	6.34E-24
60	894.746	5.38E-21	2.47E-25
61	894.806	2.61E-21	4.71E-25
62	894.920	9.17E-21	9.86E-25
66	895.154	4.50E-21	4.38E-25
67	895.203	5.16E-21	3.00E-25
68	895.252	1.24E-21	5.77E-25

and those given in Table 2 are the rigorous ones only from the ab initio data. We have singled out these transitions in italic in Table 2. Finally, it is worth noting that some of the identified lines are in fact ro-vibrational: we have excluded these transitions from our sensitivity analysis (see next section and Table 3).

3.1 Temperature-sensitive water lines: a theoretical study

Once the water lines have been assigned, we attempt to determine the sensitivity of each pure rotational transition to small (25 K) changes in temperature. This can be determined by simply estimating the *relative* intensity of the lines as a function of temperature by the use of modified Boltzmann equation:

$$I_{\rm rel} \sim 10^{-15} \frac{g_{\rm lower}}{U} \exp\left(-\frac{E_{\rm lower}}{kT}\right),$$

where $g_{\rm lower}$ and $E_{\rm lower}$ are, respectively, the statistical weight and the energy level for the lower rotational state, and U is the total partition function (which is a function of the temperature, T). Note that our choice of 25 K is rather arbitrary: in order to use pure rotational water lines as good tools for the determination of the effective temperature of LMS, we require these lines to be sensitive to temperature changes below the temperature discrepancy found by other methods, usually at least 100 K. We calculated the partition function using the fitting formula of Harris et al. (1998) (equation 12) which is suitable for high temperatures. We have considered temperatures ranging from 1500 to 4000 K in steps of 25 K. Examples of intensities and gradients versus temperature are given in Fig. 5 for two pure rotational water transitions: while the weak water transition at 797.424 cm^{-1} (line 5 from Table 2) exhibits a fairly low and flat gradient, the water transition at 894.637 cm^{-1} (line 58 from Table 2) is very sensitive to temperature changes up to ∼2800 K but it becomes less sensitive at higher temperatures. The temperature of the maximum gradient (i.e. the temperature at which the transition is most sensitive to temperature changes) for all lines is also given in Table 2 (last column). We find that about 10 transitions out of the 36 pure rotational ones identified in the BT2 linelist are sensitive enough to small (25K) temperature changes that they could potentially be used in the determination of an effective temperature scale for LMS. Clearly, a 25 K sensitivity is a strict requirement. A 50 K sensitivity would still make our methodology more accurate than others and would lead to the use of a larger number of lines: from the 36 pure rotational ones identified here we find about 14.

The use of the most temperature-sensitive water transitions for the determination of an accurate effective temperature scale of LMS becomes practical once a range of calibration objects has been observed with suitable measurements of water transitions. Our two dwarf stars only span around 300 K and have inadequate S/N for these purposes. Nevertheless, we attempt here to demonstrate the methodology by computing the intensity and gradient of the *pure rotational* transitions from Table 2 at 3500 K. Our computations are shown in Table 3 which includes the subset of rotational lines and are identifiable in the sunspot atlas. From this table, we see that some of the most sensitive lines, at this particular temperature, are around 894.6 cm^{-1}. In Fig. 6, we plot the ratio of the two stellar spectra for a small wavelength region centred at 894.6 cm^{-1} and compare it to the ratio of two synthetic spectra computed at 3200 and 3500 K. The strength of the 'absorption' for some of the lines in the divided spectra is a clear indication that the transitions identified from Table 3 are indeed the most sensitive to temperature variations. It should be noted that the strongest most sensitive water lines occur towards lower temperatures. Observations of cooler objects should be within the reach of instruments such as Echelon-Cross-Echelle Spectrograph on Stratospheric Observatory for Infrared Astronomy. The method can be calibrated with measurements of the growing number of cool low-mass eclipsing binaries.

Finally, an effective temperature scale for LMS can only be quantitatively derived if effects such as stellar rotation, internal and atmospheric structure and equation of state are taken into consideration when generating the synthetic spectra.

4 CONCLUSIONS

In this paper, we present the first high-resolution MIR spectra of M dwarfs. Very high resolution observations of pure rotational water vapour transitions in the MIR may provide us with a new methodology in the determination of the effective temperatures for LMS. We have used the latest state-of-the-art water linelist (BT2; Barber et al. 2006) to identify and assign water transitions in these spectra. In total, we assign 52 water lines out of 71 likely water transitions; 36 are pure rotational lines. We have computed a theoretical sensitivity study to determine how sensitive each pure rotational water transition is to small (25 K) changes in effective temperature and

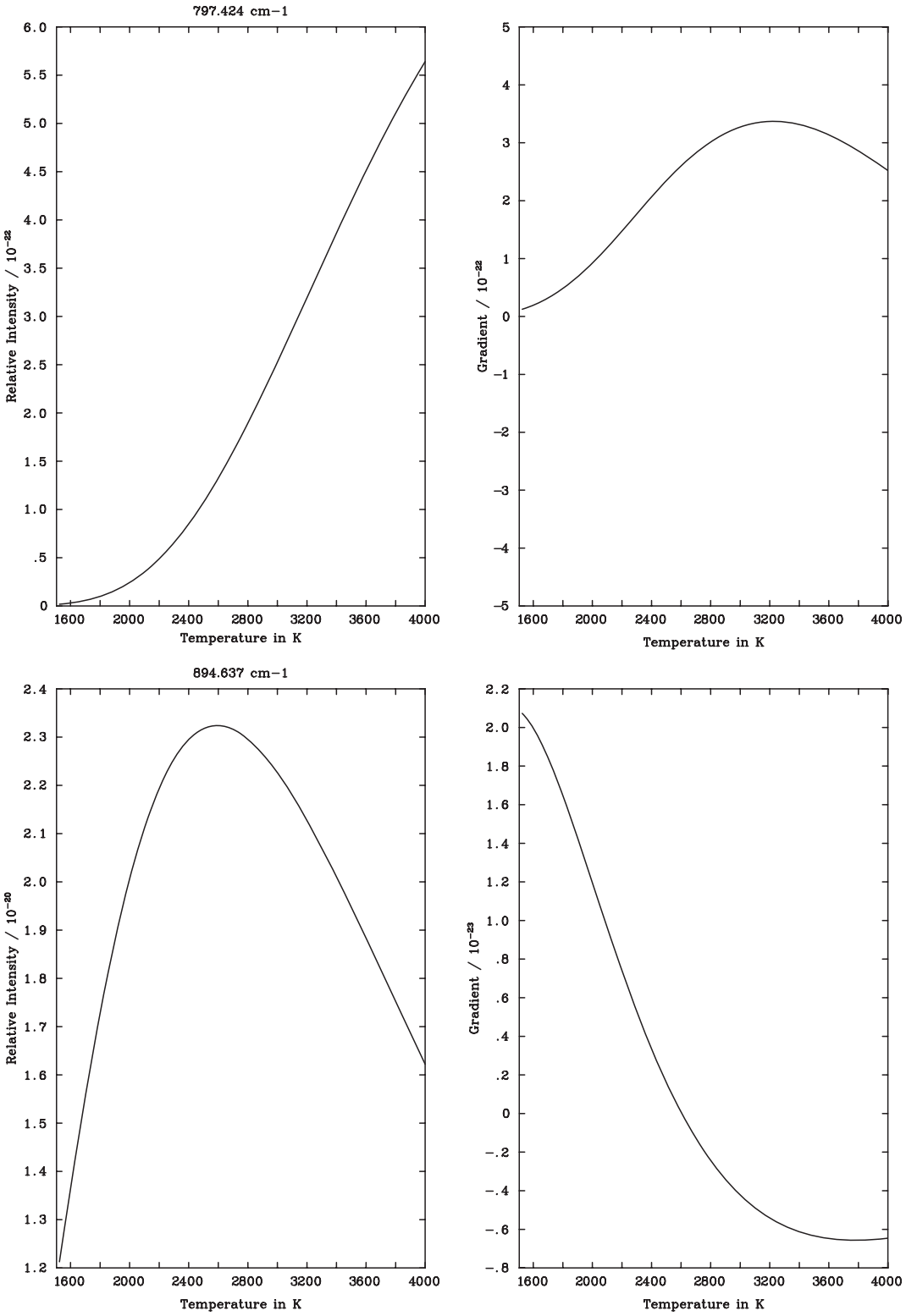

Figure 5. Relative intensity (e.g. Column 2 in Table 2) versus temperature (left-hand side) and actual gradient versus temperature (right-hand side) for a weak (top) and a strong (bottom) pure rotational water transitions from Table 3. The top gradient has been multiplied by a factor of 10^3 to fit within the same scale as the bottom one.

we find that at least 10 should be sensitive enough to be used as temperature indicators.

Due to the small wavelength region observed, the lack of a statistical sample of objects spanning lower temperatures and the low S/N, it is impossible at this stage to determine the effective temperature of our two M dwarfs using the methodology outlined in this work; our technique is viable only provided we have a large enough number of sensitive rotational lines (hence a larger number

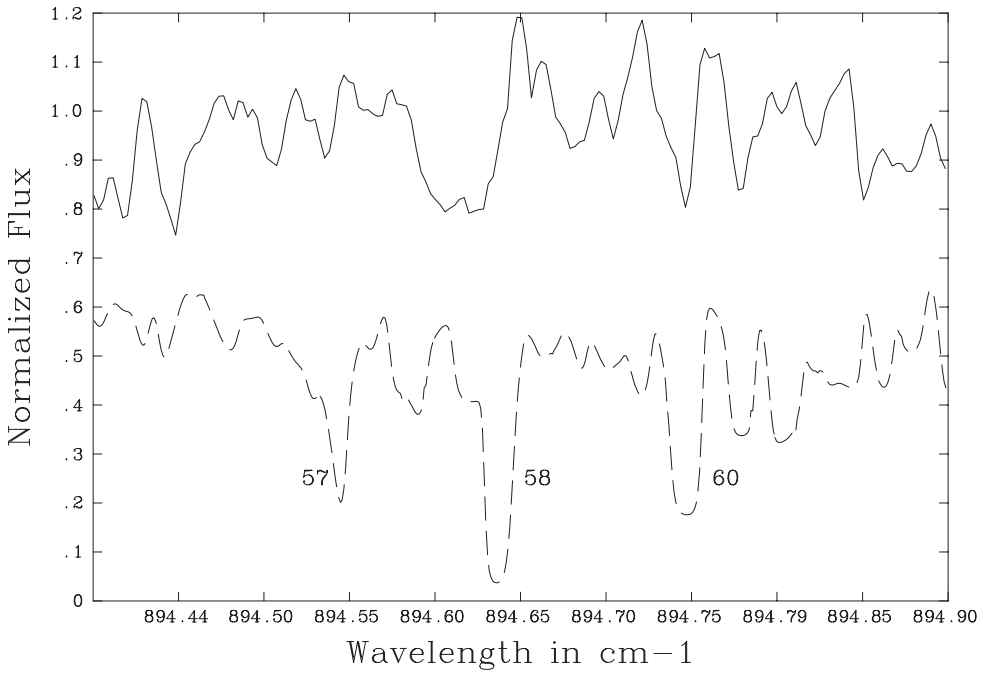

Figure 6. Ratio of the GJ273 and GJ411 spectra (top) compared to a ratio of two synthetic spectra computed using the BT2 water linelist, at 3200 and 3500 K.

of wavelength regions in the 8–21 μm spectrum), as well as a large sample of objects spanning the cool spectral subsequences. Both TEXES on Gemini and future generation telescopes such as the ELT have the potential to achieve this.

Besides the need of a larger sample of objects, ultimately, for a realistic determination of an effective temperature scale, model atmospheres including the BT2 water linelist should be used for future analysis.

ACKNOWLEDGMENTS

Based on observations obtained at the Gemini Observatory, which is operated by the Association of Universities for Research in Astronomy, Inc., under a cooperative agreement with the NSF on behalf of the Gemini partnership: the National Science Foundation (United States), the Science and Technology Facilities Council (United Kingdom), the National Research Council (Canada), CONICYT (Chile), the Australian Research Council (Australia), CNPq (Brazil) and SECYT (Argentina). Observations with TEXES (GN-2006B-Q-49) were supported by NSF grant AST-0607312. SV acknowledges financial support from an individual PPARC Advanced Fellowship. MJR acknowledges NSF grant AST-0708074. We thank the referee for constructive comments which helped to improve the manuscript.

REFERENCES

Allard F., Hauschildt P. H., Alexander D. R., Starrfield S., 1997, ARA&A, 35, 137
Allard F., Hauschildt P. H., Schwenke D., 2000, ApJ, 540, 1005
Barber R. J., Tennyson J., Harris G. J., Tolchenov R. N., 2006, MNRAS, 368, 1087
Coheur P.-F. et al., 2005, J. Chem. Phys., 122, 74307
Cushing M. C., Rayner J. T., Vacca W. D., 2005, ApJ, 623, 1115
Delfosse X., Forveille T., Perrier C., Mayor M., 1998, A&A, 331, 581
Fluks M. A., Plez B., The P. S., de Winter D., Westerlund B. E., Steenman H. C., 1994, A&AS, 105, 311
Harris G. J., Viti S., Mussa H. J., Tennyson J., 1998, J. Chem. Phys., 109, 7197
Jones H. R. A., Longmore A. J., Allard F., Hauschildt P. H., 1996, MNRAS, 280, 77
Jones H. R. A., Pavlenko Y., Viti S., Tennyson J., 2002, MNRAS, 330, 675
Jones H. R. A., Pavlenko Y., Viti S., Barber R. J., Yakovina L. A., Pinfield D., Tennyson J., 2005, MNRAS, 358, 105
Lacy J. H., Richter M. J., Greathouse T. K., Jaffe D. T., Zhu Q., 2002, PASP, 114, 153
Leggett S. K., Allard F., Dahn C., Hauschildt P. H., Kerr T. H., Rayner J., 2000, ApJ, 535, 965
Leggett S. K., Allard F., Geballe T. R., Hauschildt P. H., Schweitzer A., 2001, ApJ, 548, 908
Marcy G. W., Lindsay V., Wilson K., 1987, PASP, 99, 490
Partridge H., Schwenke D. W., 1997, J. Chem. Phys., 106, 4618
Polyansky O. L., Zobov N. F., Viti S., Tennyson J., Bernath P. F., Wallace L., 1997a, Sci, 277, 346
Polyansky O. L., Zobov N. F., Viti S., Tennyson J., Bernath P. F., Wallace L., 1997b, ApJ, 489, L205
Ryde N., Richter M. J., Harper G. M., Eriksson K., Lambert D. L., 2006, ApJ, 645, 652
Tsuji T., Ohnaka K., Aoki W., 1996, A&A, 305, L1
Wallace L., Bernath P., Livingston W., Hinkle K., Busler J., Guo B., Zhang K., 1995, Sci, 268, 1155
Zobov N. F., Shirin S. V., Polyansky O. L. et al., 2006, J. Molec. Spectrosc., 237, 115

This paper has been typeset from a TEX/LATEX file prepared by the author.